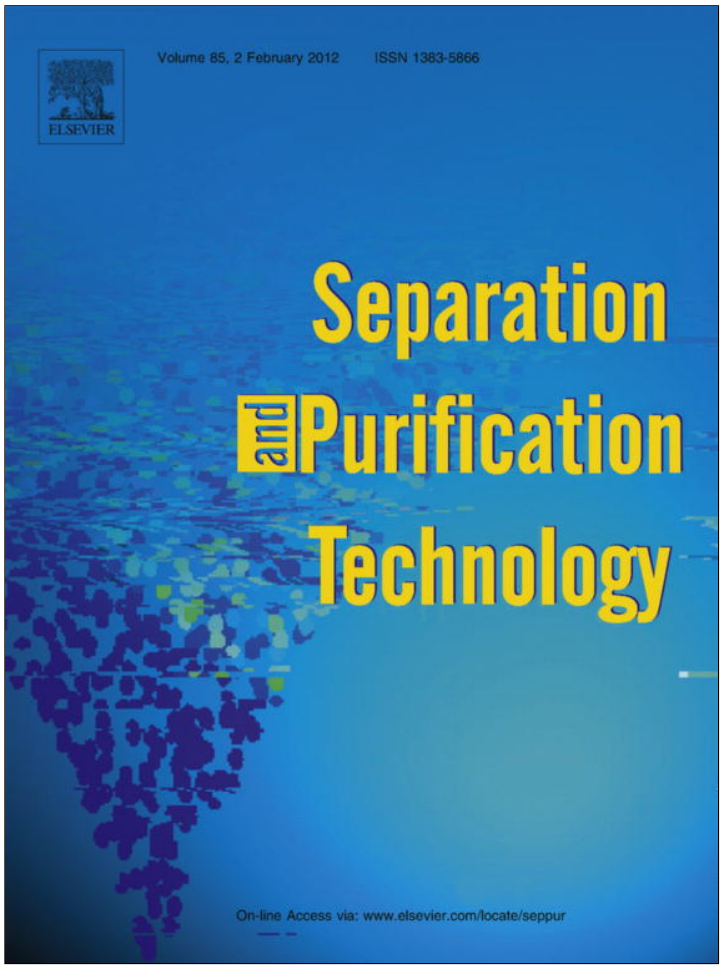

(This is a sample cover image for this issue. The actual cover is not yet available at this time.)

Separation and Purification Technology 98 (2012) 488–496

Contents lists available at SciVerse ScienceDirect

Separation and Purification Technology

journal homepage: www.elsevier.com/locate/seppur

A study on the degradation efficiency and mechanisms of ethyl violet by HPLC–PDA–ESI–MS and GC–MS

Wenlian-William Lee [b], Wen-Hsin Chung [c], Chung-Shin Lu [d], Wan-Yu Lin [c], Chiing-Chang Chen [a,*]

[a] Department of Science Application and Dissemination, National Taichung University of Education, Taichung 403, Taiwan, ROC
[b] Department of Occupational Safety and Health, Chung-Shan Medical University, Taichung 402, Taiwan, ROC
[c] Department of Plant Pathology, National Chung Hsing University, Taichung 402, Taiwan, ROC
[d] Department of General Education, National Taichung University of Science and Technology, Taichung, Taiwan, ROC

ARTICLE INFO

Article history:
Received 26 January 2011
Received in revised form 6 June 2012
Accepted 12 June 2012
Available online 30 June 2012

Keywords:
HPLC–PDA–ESI–MS
GC–MS
EV dye
Zinc foil
Degradation mechanism

ABSTRACT

This study employed HPLC–PDA–ESI–MS analysis to characterize the mechanisms underlying the degradation of ethyl violet dyes. A nanostructural ZnO film was fabricated on the surface of the Zn foil of Alkaline-Manganese dioxide–Zinc Cells through a simple oxidation reaction in aqueous solution at room temperature. Our results indicate that the ZnO nanostructure/Zn-foil has outstanding potential for future applications in the photocatalytic degradation of organic dyes. The nanostructural polycrystalline ZnO was characterized using XRD, SEM, and XPS. To identify the underlying mechanism involved in ZnO/Zn-assisted degradation of EV dye, we separated and characterized 26 intermediates using HPLC–PDA–ESI–MS and GC–MS. Specifics related to the quantities of the intermediates provide an indication of possible degradation pathways associated with the decolorization of EV dyes.

1. Introduction

It is estimated that the worldwide production of dyes and pigments exceeds 700,000 tons annually, 20% of which are utilized for textile dyeing and finishing processes [1]. Due to their complex polyaromatic structures, many of these synthetic dyestuffs cannot be removed through conventional treatment, which poses a serious threat to the environment [2]. The textile, paper, food, cosmetic, and leather industries are major consumers of triphenylmethane dyes [1,2]. Previous reports [3,4] have shown that triphenylmethane dyes containing *N*-alkylamine groups can be photodegraded through consecutive *N*-dealkylation reaction. Others have reported that thyroid peroxidase-catalyzed oxidation of triphenylmethane dyes could result in the formation of various *N*-de-alkylated primary and secondary aromatic amines, which possess structures similar to those of aromatic amine carcinogens [5]. Previous studies on the photocatalytic degradation of nitrogen-containing aromatic compounds have demonstrated that both electrons and hydroxyl radicals transformed the amine functional groups [6,7].

Zinc oxide has attracted considerable interest for its applicability in photocatalysis [3], piezoelectricity, field emissions, and lasing action [8,9]. Recently, various synthetic methods have been developed for the production of nanostructural ZnO, including hydrothermal, vapor–liquid–solid, vapor solid, and other solution processes [10–19]. One low-temperature chemical–liquid deposition method has been developed to grow oriented ZnO nanorods by supplying Zn ions from a Zn foil to form a ZnO thin film in an aqueous formaldehyde solution [20]. A similar reaction using Zn^{2+} salt with ethanol in the presence of amine produces one-dimensional nanostructures of ZnO [21]. Hydrothermal reactions have been applied been to the preparation of the ZnO nanorods, in which zinc acetate was dissolved in ethanol with polyvinylpyrrolidone and NaOH [22]. Heating zinc nitrate and NaOH in a mixture of ethylenediamine and water at 180 °C for 20 h also produced ZnO nanorods [23]. Another approach involves the reaction of Zn foil with water, in the presence of ethylenediamine, under hydrothermal conditions (150–230 °C) [24–27,13]. At room temperature, the natural oxidation of zinc metal by dissolved oxygen in water is rather slow due to the existence of a surface oxide layer. However, with dye solutions, this spontaneous oxidation reaction can be accelerated considerably, enabling the generation of ZnO nanoclusters on the surface of the zinc foil. The reaction between Zn and O_2 in an aqueous solution is generally recognized to produce ZnO, as shown in the following equations:

$$Zn \rightarrow Zn^{2+} + 2e^- \quad E^\circ = 0.76\ V \tag{1}$$

$$1/2O_2 + H_2O + 2e^- \rightarrow 2OH^- \quad E^\circ = 0.80\ V \tag{2}$$

* Corresponding author. Tel.: +886 422183406; fax: +886 422183560.
E-mail address: ccchen@mail.ntcu.edu.tw (C.-C. Chen).

1383-5866/$ - see front matter © 2012 Elsevier B.V. All rights reserved.
http://dx.doi.org/10.1016/j.seppur.2012.06.020

$$Zn^{2+} + 2OH^- \rightarrow ZnO + H_2O \quad E^\circ = 0.49\ V \tag{3}$$

$$Zn + 1/2O_2 \rightarrow ZnO \quad E^\circ = 2.05\ V \tag{4}$$

Recent research has revealed that the single C–O bond of aliphatic alcohols is readily cleaved on zinc metal surfaces, resulting in the production of ZnO nanoparticles [28]. Unfortunately, most of these methods require high temperatures. The reaction of Zn metal with liquid water can also produce ZnO nanostructures, based on the evolution of hydrogen in acidic conditions [29,30]. Most methods adopting this approach have used amines and other additives or zinc compounds under higher temperature conditions. Encouraged by these results, the reaction of Zn metal with ethyl violet dye in aqueous solutions has also been examined. This study proposes a simple method of producing ZnO nanostructures to decompose ethyl violet dye through a reaction with metals in liquid water. To the best of our knowledge, this simple method has not been previously reported.

This study selected zinc foil obtained from wasted Alkaline-Manganese dioxide–Zinc Cells as a substrate for the generation of ZnO nanostructures, due to the matching of lattices between ZnO and Zn crystals, which facilitates the generation of the ZnO nanostructure. In addition, zinc foil from these cells is a waste material ideally suited to the treatment of organic wastewater through photocatalysis. Zinc foil serves as both reactant and substrate to support the ZnO nanostructures without the need for an additional substrate or high temperatures. This method is a simple, economical solution to the treatment of organic wastewaters.

In short, this study reports a simple solution-based approach to the fabrication of ZnO nanostructures on zinc foil. We also employed HPLC–ESI–MS and GC–MS to identify the reaction intermediates to gain an understanding of the mechanisms involved in the degradation of EV dyes. It is hoped that these results will provide a foundation for the future development of environmental solutions.

2. Experimental section

2.1. Materials and reagents

The Zn foils were 0.15 m long, 0.150 m wide, and 2.5×10^{-4} m thick with a purity of 99.9%. Alkaline-Manganese dioxide–Zinc Cells were obtained from Eveready, Toshiba, and Panasonic. Ethyl violet dye was obtained from Tokyo Kasei Kogyo Co. The chemical structure of EV is shown in Fig. 1. 4-Aminophenol (AP; analytical standard) was purchased from Riedel–deHaen. Reagent-grade ammonium acetate, nitric acid, sodium hydroxide, hydrogen chloride, and HPLC-grade methanol and acetone were purchased from Merck. All the above agents were used as received, without further purification.

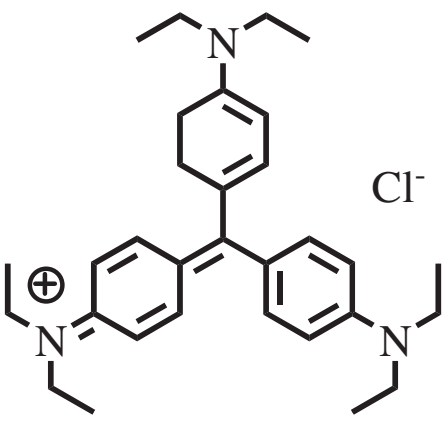

Fig. 1. Chemical structure of EV.

2.2. Degradation experiments

The Zn foils were ultrasonically washed with HPLC-grade acetone three times prior to use. A mixture solution was prepared by adding Zn foil (0.05 m × 0.05 m) to a 0.25 L aqueous solution containing EV in appropriate concentrations. The initial pH of the solution was adjusted by adding either NaOH or HNO_3 solution. At given intervals in the reaction, the solution was sampled. Analysis of the residual dye and organic intermediates was performed by HPLC–PDA–ESI–MS and GC–MS. Dark experiments performed in the beaker also showed decolorization of the dye solution. For comparison, irradiation experiments were carried out using 15 W lamps to determine the expected stability of EV dye under UV or visible light irradiation. The 0.01 g L^{-1} EV solutions did not demonstrate significant de-coloration under UV irradiation without Zn foil. Following the reactions, the Zn foil was removed, washed with de-ionized water and ethanol several times, and then dried with nitrogen. These Zn foils were characterized using X-ray diffraction (XRD), field emission scanning electron microscopy (FE-SEM), and high resolution X-ray photoelectron spectrometry (HRXPS).

2.3. Instruments and analytical methods

XRD patterns were recorded on a MAC Science, MXP18 X-ray diffractometer with Cu Kα radiation, operated at 40 kV and 0.08 A. FE-SEM measurement performed using a field-emission microscope (JEOL JSM-7401F) operated at an acceleration voltage of 1.5×10^4 V. HRXPS measurement was carried out using ULVAC-PHI XPS: PHI Quantera SXM to measure changes in the surface structure following reflux treatment. XPS spectra were collected by exciting the film without pre-treatment using an Al Kα X-ray source. Al Kα radiation was generated at a voltage of 1.5×10^4 V. The spectrometer was calibrated with an Ag $3d^{5/2}$ core line. The binding energy values reported in the present work were corrected to C 1s peak at 284.8 eV to take charging effects into account.

A Waters ZQ LC/MS system, equipped with Waters 1525 Binary HPLC pumps, a Waters 2998 Photodiode Array Detector, a Waters 717 plus auto sampler, and a Waters micromass-ZQ 2000 detector, was used. The analysis of organic intermediates was performed using HPLC–PDA–ESI–MS following the readjustment of the chromatographic conditions to make the mobile phase compatible with the working conditions of the mass spectrometer. Two types of eluent were employed in this study: solvent A comprised 0.025 M aqueous ammonium acetate buffer (pH 6.9) and solvent B was methanol. LC was performed on an Atlantis™ dC18 column (0.25 m × 0.046 m i.d., 5×10^{-6} m film thickness). The flow rate of the mobile phase was set at 0.001 L min^{-1}. The column effluent was introduced into the ESI source of the mass spectrometer.

Solid-Phase Extraction (SPE) was employed for the pre-concentration of irradiated samples prior to GC–MS analysis. GC/MS analysis was performed on a Perkin–Elmer AutoSystem-XL gas chromatograph interfaced to a TurboMass selective mass detector. Separation was carried out in a DB-5 capillary column (5% diphenyl/95% dimethyl-siloxane) with an inside diameter of 60 m, 2.5×10^{-4} m, and film thickness of 1.0×10^{-6} m. Electron Impact (EI) mass spectra were monitored from 35 to 300 m/z. The ion source and inlet line temperatures were set at 220 and 280, respectively.

3. Results and discussion

3.1. Characterization of material

3.1.1. FE–SEM–EDS

Supporting material, Figs. S1 and S2, present SEM images of the ZnO nanostructures and microcrystals formed on the surface of the

Zn foil. The diameter of the ZnO formations increased with reaction time. Fig. S1 presents a top-down image of the rods (polycrystallines) with sizes of approximately 0.2–1 $\times 10^{-7}$ m in diameter and 1.5–3 $\times 10^{-7}$ m in length and microcrystalline sizes of approximately 3–5 $\times 10^{-6}$ m in diameter. The composition of the rods was characterized using energy dispersive spectroscopy (EDS), which revealed Zn and O as the only elementary components with oxygen deficiencies (Zn:O ~ 2:1 atomic ratio) [31]. Fig. S2 shows the growth of ZnO film on various Zn foils.

3.1.2. XRD

Fig. 2 presents XRD patterns of the ZnO sample prepared in DI water at room temperature with/without irradiation. All of the absorption peaks correspond well with ZnO (JCPDS card no. 36-1451) and Zn (JCPDS card no. 4-831). No obvious diffraction pattern was observed for the impurities. The characteristic diffraction pattern of ZnO (100), (002), and (101), appeared with the diffraction pattern of Zn (002), (100), and (101) in all samples.

3.1.3. XPS

Fig. 3 shows the XPS spectra of ZnO samples obtained under various conditions. The binding energies of O1s in all samples were within 529.1–531.1 eV, which further confirmed the presence of Zn^{2+} and O^{2-} in all samples.

3.2. Degradation of EV by ZnO foil

3.2.1. Control experiments

Fig. 4 presents kinetic data typical of the effects of photo irradiation. Under completely dark conditions, approximately 80% of the EV dye was degraded on the Zn surface after 8 h. In addition, the results of the photo irradiation experiments demonstrated that, under visible light conditions, the concentration of EV dye decreased by 93% after 8 h irradiation; under UV irradiation, nearly 96% amount of the EV dye was removed after 8 h. The dark (control) experiments indicate that the EV dye might have been degraded by Zn through reduction reaction and the presentation of ZnO film was the resulting product indicated by the SEM and the XRD characterization data, which further proceeded photocatalytic reaction under photo-irradiation reaction conditions. It has been reported that ZnO-assists the photocatalytic degradation of the triphenylmethane dye under UV-365 nm and visible light irradiation [3,23]. This study clearly revealed that both Zn and ZnO degrade EV dye, mostly through the reduction of Zn; however, under photo-irradiation conditions, the ZnO acts as a photocatalyst, thereby contributing significantly to the degradation of EV dye.

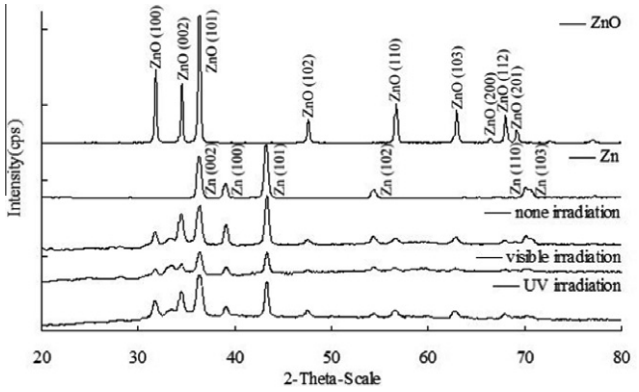

Fig. 2. The XRD patterns of ZnO/Zn film in DI water under UV and visible irradiation for 64 h.

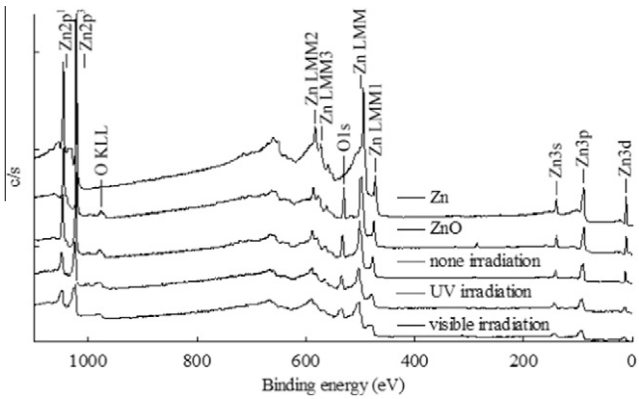

Fig. 3. The XPS spectra of ZnO/Zn film in DI water under UV and visible irradiation for 64 h.

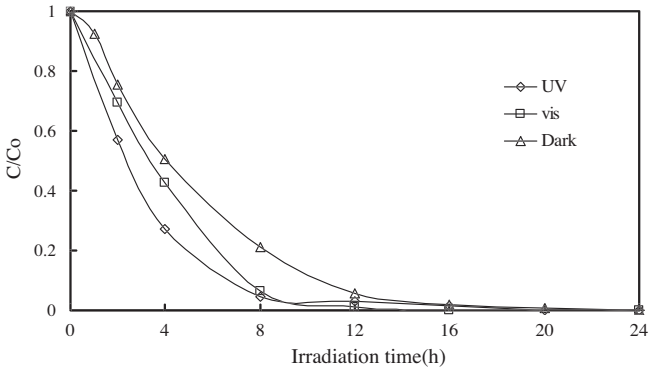

Fig. 4. The direct degradation of EV at dark and different wavelength irradiation: 365 nm and visible light. (EV = 10 ppm, pH = 6, Zn foil = 5 × 5 cm^2).

3.2.2. Influence of pH

The degradation rate of EV dye as a function of pH without UV irradiation is shown in Fig. 5. The degradation rate remained constant as the pH value of the solution increased. A reduction in the degradation rate is clearly observable at pH 3, which could be attributed to the reaction of zinc metal with protons, resulting in the slow production of hydrogen gas. It has been previously reported that Zn metal under acidic water conditions could result in the formation of ZnO film associated with the evolution of hydrogen [28].

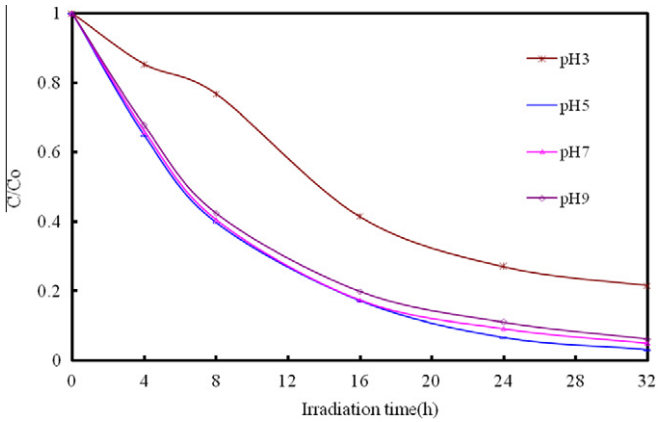

Fig. 5. pH effect on the EV degradation rate: Zn foil of Alkaline-Manganese dioxide–Zinc Cell; EV = 10 ppm; without UV irradiation.

3.2.3. Reusability of Zn-foil

The reusability of Zn-foil was evaluated by preparing fresh and reused Zn-foil as reactants, under the same processing conditions, and recording the degradation efficiency. As shown in Fig. 6, the degradation efficiency of reused Zn-foil is lower than that of fresh Zn-, which could be attributed to of the decreased number of active sites on the surface of reused Zn-foil. As indicated in Fig. 6, degradation efficiency was unaffected by the number of times the Zn-foil was reused. This can be explained by the fact that ZnO was formed and continuously peeled off the Zn-foil surface, leaving ZnO powders following the reaction, as shown in the SEM images obtained between 8 and 64 h of irradiation (Fig. S2).

3.2.4. Influence of EV dye concentration

In textile effluent, dye concentrations typically range between 150 and 200 ppm. By varying the initial dye concentrations from 10 to 200 ppm, with constant Zn-foil loading (pH = 6), the influence of dye concentration on the degradation rate was determined, and the results are shown in Fig. S3. Degradation efficiency is inversely affected by dye concentration. This negative effect can be explained by the fact that, as the dye concentration increased, the equilibrium adsorption time of dye on the surface of the Zn-foil active sites also increased; hence the competitive adsorption of O_2 on the same sites decreased, which lowered the rate of ZnO formation and subsequently decreased EV dye degradation efficiency.

3.3. Separation of the intermediates

Fig. 7 presents chromatograms recorded at 580, 350, and 300 nm. With a UV irradiation time of up to 36 h at pH 6, 21 components were identified within a 50 min retention time. The EV dye and its related intermediates as species are denoted as A–J, a–f, a′–b′, and α–γ. With the exception of the initial EV dye (peak A), all of the peaks initially increased before subsequent decreasing, indicating the formation and the transformation of the intermediates. Fig. 8 shows the GC chromatogram obtained from an SPME extract of EV solution after 36 h of photo-irradiation reaction. Six compounds were identified as possible degradation intermediates. These intermediates are denoted as compounds **I**–**VI**.

3.4. Identification of the intermediates

3.4.1. UV–visible spectra of the intermediates

The UV-PDA adsorption spectra of the intermediates are depicted in Supplementary material Fig. S4, identified as A–J and a–f, corresponding to the peaks A–J and a–f, in Fig. 7, respectively. The maximum absorption of the spectral band shifted from 591.8 nm (spectrum A) to 561.7 nm (spectrum I), and from 371.6 nm (spectrum a) to 340.6 nm (spectrum f). Presumably,

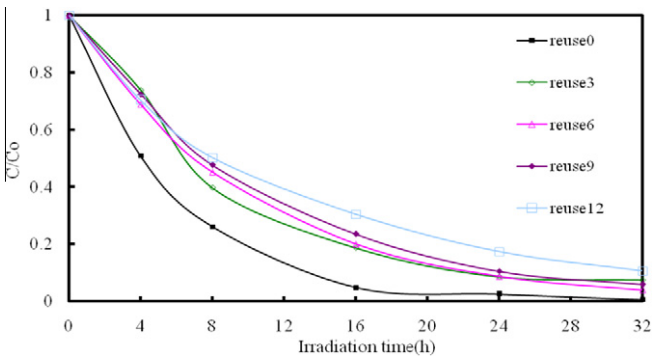

Fig. 6. Comparison of degradation rate for the degradation of EV under Zn foil of Alkaline-Manganese dioxide–Zinc Cell and reused Zn foil (10 ppm, pH = 6).

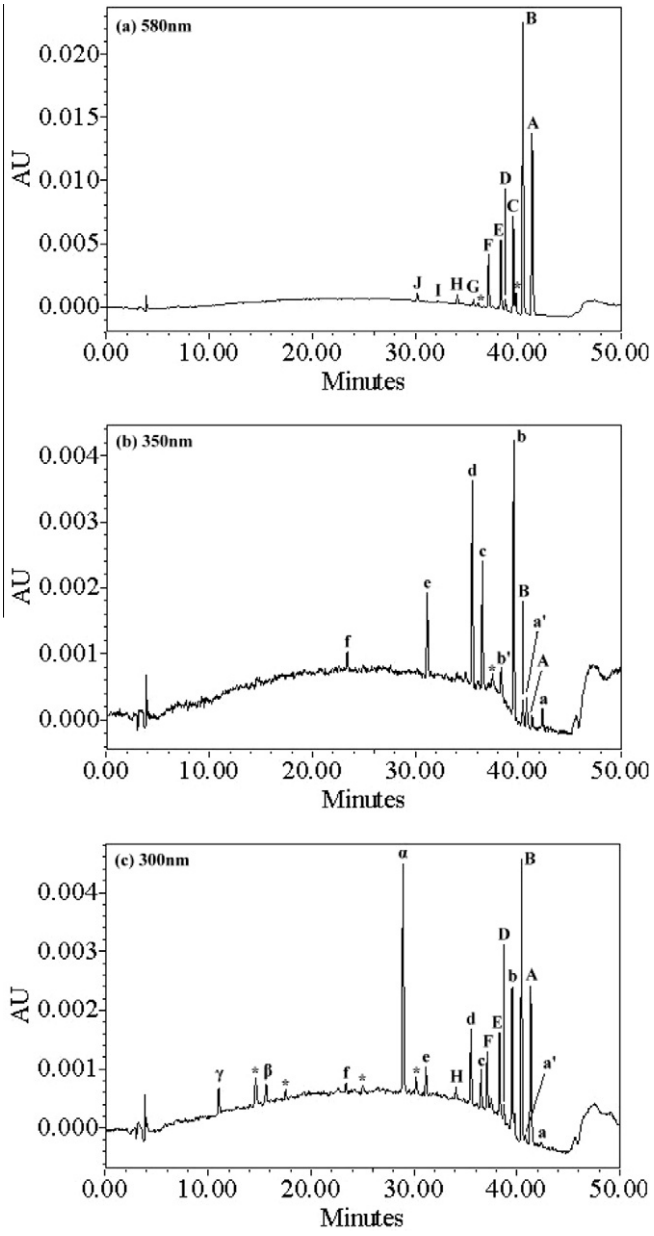

Fig. 7. HPLC chromatogram of intermediates at pH 6 (EV, 0.01 g L^{-1}), 36 h of reaction with Zn-foil, recorded at (a) 580 nm, (b) 350 nm, and (c) 300 nm, impurities were marked with star.

these shifts are due to the formation of a series of *N*-de-ethylated and *N*-hydroxyethylated intermediates. From these results, several groups of intermediates were distinguished.

The first group is marked in the chromatogram and illustrated in Fig. 7a. The wavelength position of the major absorption bands associated with the intermediates of *N*-de-ethylated EV dye moved toward the blue region, λ_{max}, A (EV), 591.8 nm; B, 585.6 nm; C, 571.9 nm; D, 573.2 nm; E, 582.1 nm; F, 569.7 nm; G, 565.6 nm; H, 563.6 nm; I, 561.7 nm. The *N*-de-ethylation of the EV dye causing the shift in wavelength is depicted in Fig. S4 as an attack by active oxygen species on the *N*,*N*-diethyl or *N*-ethyl group. It has been reported [32] that EV dye is *N*-de-ethylated in a stepwise manner (i.e., ethyl groups are removed stepwise, as confirmed by the blue shift in the maximum absorbance associated with separated intermediates.

The second and third groups are marked in the chromatogram and illustrated in Fig. 7b. The destruction of EV yielded DAP, DDBP,

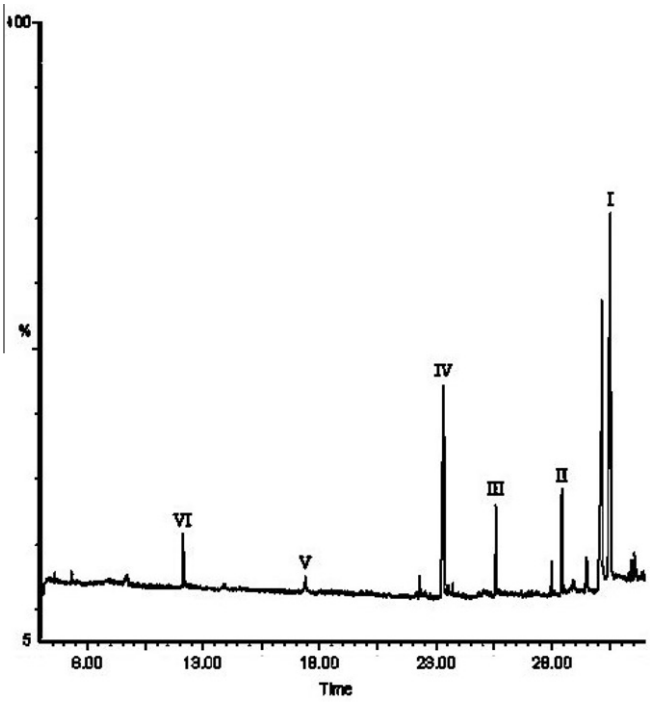

Fig. 8. GC–MS/EI chromatogram obtained for a SPE extract of solution after 36 h of EV dye with Zn-foil under dark condition.

and their *N*-de-ethylated products, *N*-hydroxyethylated intermediates. The *N*-de-ethylation derivatives of the DDBP and the *N*-hydroxyethylated intermediates of the *N*-de-ethylated DDBP species, produced by cleavage of the EV chromophore ring structure, have their λ_{max} blue shifted to the following wavelengths: a, 371.6 nm; b, 366.7 nm; c, 365.5 nm; d, 367.9 nm; e, 352.6 nm; f, 340.6 nm. The proposed intermediate a compares well with standard material of 4-(*N*,*N*-diethylamino)-4′-(*N*′,*N*′-diethylamino) benzophenone.

The fourth and the fifth groups are marked in the chromatogram and illustrated in Fig. 7c. The *N*-de-ethylation derivatives of the DAP, produced by cleavage of the EV chromophore ring structure, have their λ_{max} blue shifted to the following wavelengths: α, 290.4 nm; β, 282.1 nm; γ, 272.6 nm, as previously reported [33].

3.4.2. Mass spectra of the intermediates

The intermediates were further identified using HPLC-ESI mass spectrometry, as illustrated in the Supplementary material Fig. S4 and further summarized in Table 1. The molecular ion peaks of the intermediates all appeared in protonated forms. The results confirm that component A (m/z = 456.49) is EV. The other components are B, m/z = 428.88; C, m/z = 400.21; D, m/z = 400.19; E, m/z = 372.16; F, m/z = 372.21; G, m/z = 344.19; a, m/z = 325.45; b, m/z = 297.48; c, m/z = 269.31; d, m/z = 269.45; e, m/z = 241.18; f, m/z = 213.13; α, m/z = 166.25; β, m/z = 137.15; γ, m/z = 109.35. The remaining intermediates are shown in the GC–MS/EI chromatogram, and the relevant mass spectra are illustrated in the Supplementary material (Fig. S5). Table 1 presents the molecular ions of the intermediates (**I**–**VI**) that characterize their corresponding structures. The peaks eluting at 30.48, 28.49, 25.61, 23.39, 17.57, and 12.38 min during GC–MS were identified as *N*,*N*-diethylaminobenzene, *N*-ethylaminobenzene, aminobenzene, acetamide, 2-propenoic acid, and acetic acid, which matched the standard library search with the values of 87%, 82%, 83%, 71%, 88%, and 95%, respectively (see Fig. S5). The intermediates identified in this study were also reported in a previous study of the MEK/TiO_2 system [33].

3.5. Degradation mechanisms of EV

Most of the EV· radicals were generated directly from the redox reaction between Zn-foil and surface-adsorbed EV dye. This was followed by an attack of H_2O on the ethyl group of diethylamine, resulting in the formation of *N*-de-ethylated intermediate and ethanol. These results can be seen more clearly in Fig. 9. The degradation reactions occurred with liquid water at the surface of the Zn metal, resulting in the production of nanostructural ZnO through

Table 1
Intermediates of the degradation of EV identified by HPLC–ESI–MS or GC–EI–MS. Conditions: Zn foil, 0.01 g L^{-1} EV, reaction 36 h.

HPLC peaks	Intermediates	Abbreviation	MS peaks (m/z)	Absorption maximum (nm)
A	*N*,*N*,*N*′,*N*′,*N*″,*N*″-hexaethylpararosaniline	EV	456.49	591.8
B	*N*,*N*-diethyl-*N*′,*N*′-diethyl-*N*″-ethylpararosaniline	DDEPR	428.88	585.6
C	*N*,*N*-diethyl-*N*′-ethyl-*N*″-ethylpararosaniline	DEEPR	400.21	571.9
D	*N*,*N*-diethyl-*N*′,*N*′-diethylpararosaniline	DDPR	400.19	573.2
E	*N*-ethyl-*N*′-ethyl-*N*″-ethyl pararosaniline	EEEPR	372.16	582.1
F	*N*,*N*-diethyl-*N*′-ethylpararosaniline	DEPR	372.21	569.7
G	*N*-ethy-*N*′-ethylpararosaniline	EEPR	344.19	565.6
H	*N*,*N*-diethylpararosaniline	DPR	N/A	563.6
I	*N*-ethylpararosaniline	EPR	N/A	561.7
J	pararosaniline	PR	N/A	N/A
a	4-(*N*,*N*-diethylamino)-4′-(*N*′,*N*′-diethylamino)benzophenone	DDBP	325.45	371.6
b	4-(*N*,*N*-diethylamino)-4′-(*N*′-ethylamino)benzophenone	DEBP	297.48	366.7
c	4-(*N*-ethylamino)-4′-(*N*′-ethylamino)benzophenone	EEBP	269.31	365.5
d	4-(*N*,*N*-diethylamino)-4′-aminobenzophenone	DBP	269.45	367.9
e	4-(*N*-ethylamino)-4′-aminobenzophenone	EBP	241.18	352.6
f	4,4′-Bis-aminobenzophenone	BP	213.13	340.6
a′	4-(*N*,*N*-diethylamino)-4′-(*N*′-hydroxyethyl-*N*′-ethylamino)benzophenone	DHEBP	341.23	371.6
b′	4-(*N*-hydroxyethyl-*N*-ethylamino)-4′-(*N*′-ethylamino)benzophenone	HEEBP	313.08	369.1
α	4-(*N*,*N*-diethylamino)phenol	DAP	166.25	290.4
β	4-(*N*-ethylamino)phenol	EAP	137.15	282.1
γ	4-aminophenol	AP	109.35	272.6
I	*N*,*N*-diethylaminobenzene	DBz	149	310.7
II	*N*-ethylaminobenzene	EBz	121	301.5
III	Aminobenzene	ABz	93	282.9
IV	Acetamide	AAm	59	N/A
V	2-Propenoic	PAc	72	N/A
VI	Acetic	AAc	60	N/A

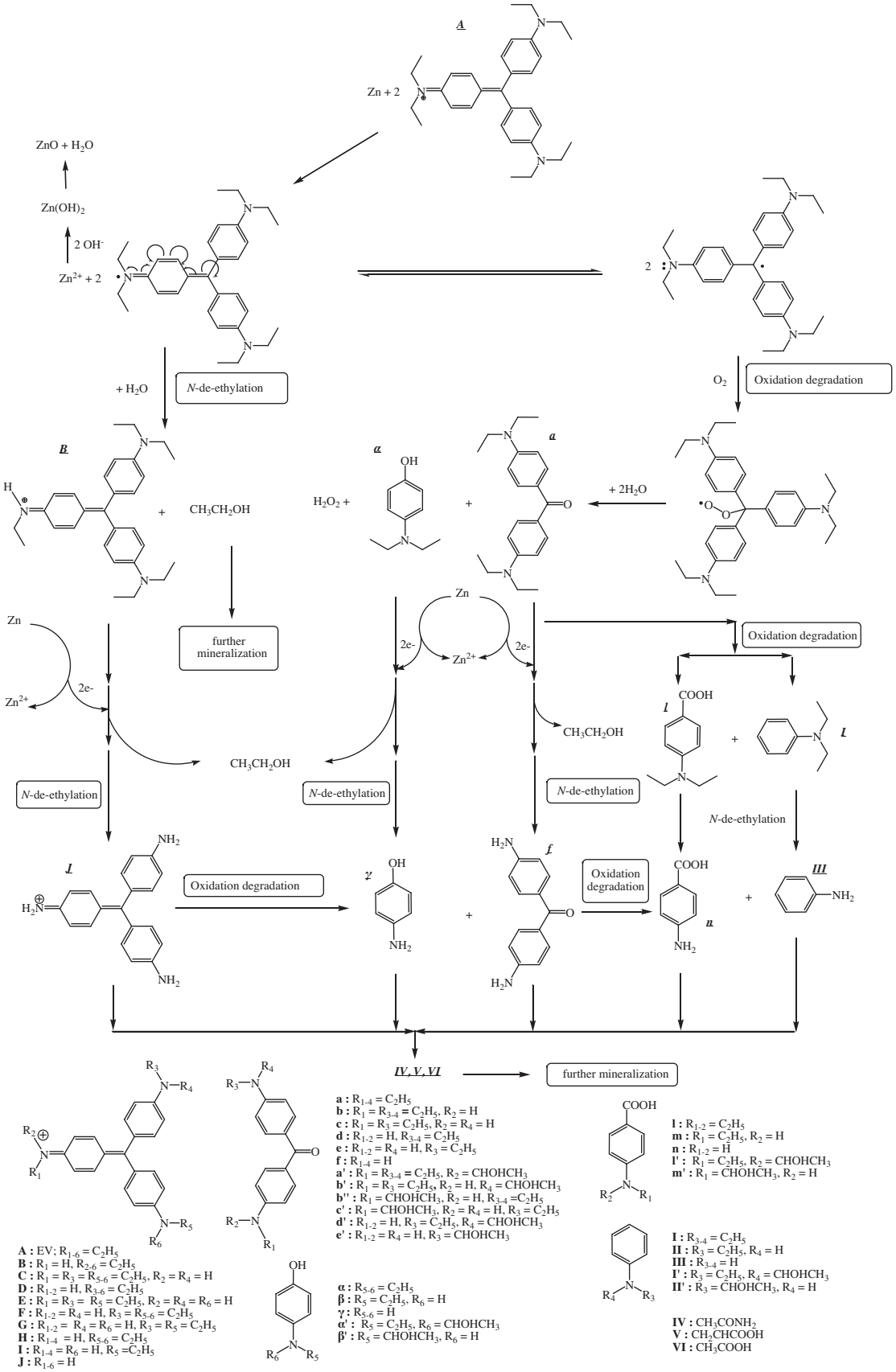

Fig. 9. Proposed reaction pathway of EV dye with Zn foil in the aqueous solution.

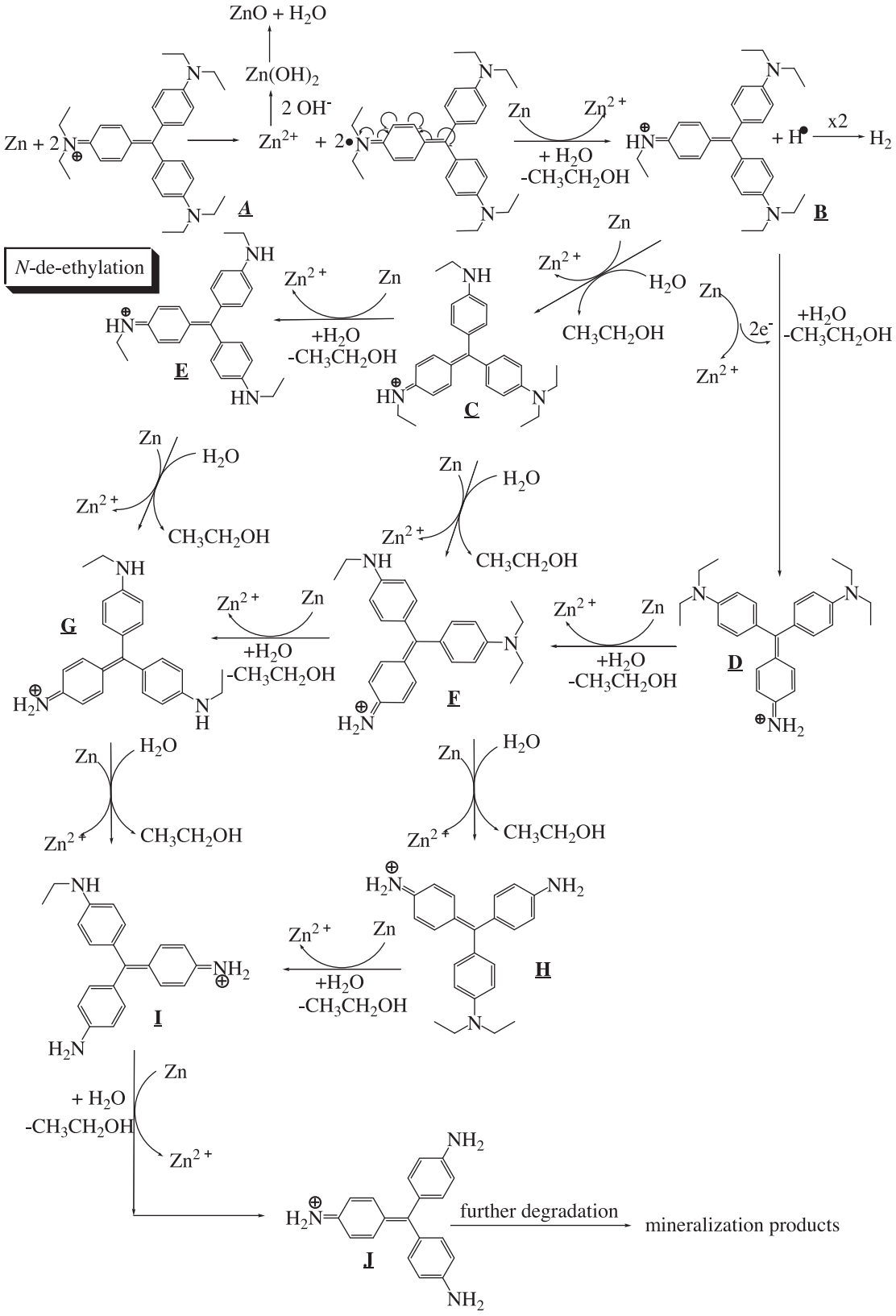

Fig. 10. Proposed *N*-de-ethylation pathway of the EV dye with Zn foil in aqueous solution followed by the identification of several intermediates by HPLC–ESI mass spectral techniques.

the evolution of hydrogen [28]. According to earlier reports [3,6], most *N*-de-alkylation processes were preceded by the formation of a nitrogen-centered radical, while the destruction of dye chromophore structures was preceded by the generation of a carbon-centered radical [3,4]. Thus, the degradation of EV must occur via two different photodegradation pathways, namely the destruction

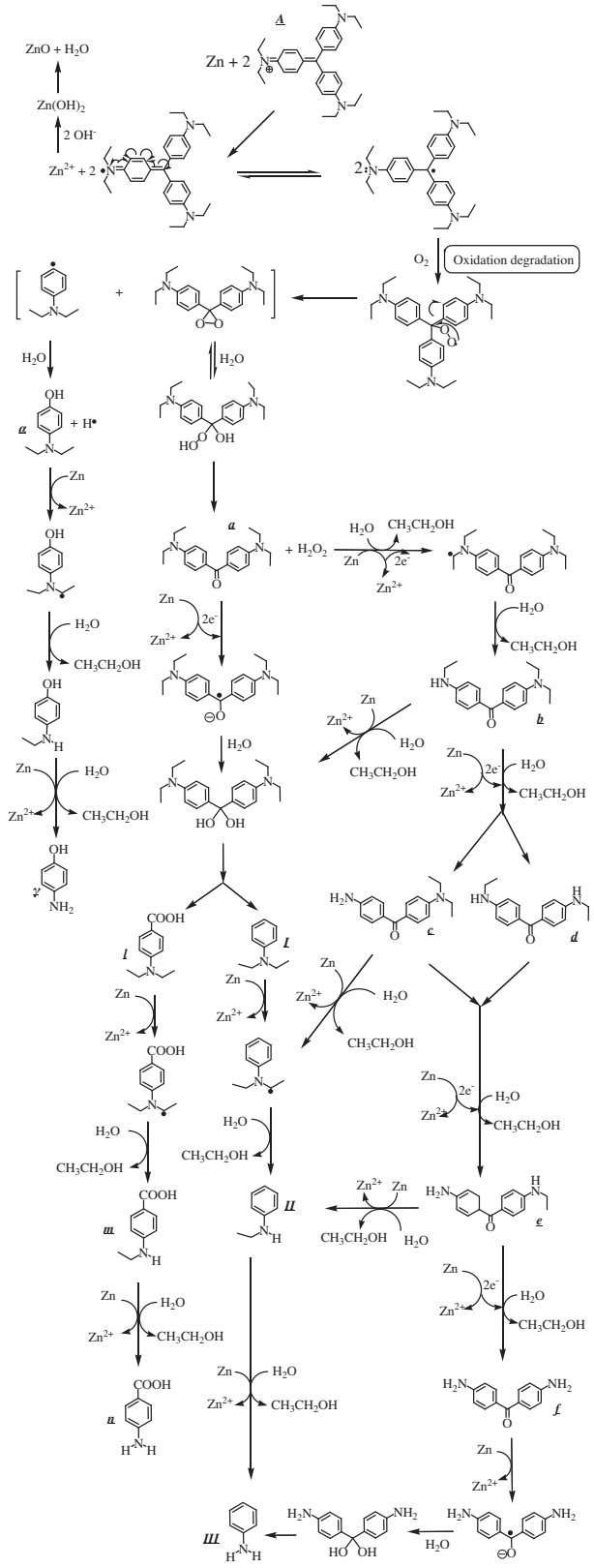

Fig. 11. Proposed pathway of the destruction of the conjugated structure of the EV dye with Zn foil followed by the identification of several intermediates by HPLC–ESI mass spectral techniques.

of the chromophore structure and *N*-de-ethylation resulting from two different radicals: either a carbon-centered or nitrogen-centered radical. There can be no doubt that the electrons from the Zn-foil attacked the dye molecules to yield a dye radical. Subsequently, the radical Dye· underwent hydrolysis and/or deprotonation, as determined by the different adsorption modes of EV on the surface of the Zn. Based on these results, the degradation pathways depicted in Fig. 9 are tentatively proposed.

3.5.1. *N*-de-ethylation of EV

EV receives an electron from the Zn surface via the positive diethylamine group to form EV· radicals and zinc ions. This is followed by one molecule of H_2O attacking the ethyl group of diethylamine on the EV· radicals, which results in the formation of *N*-de-ethylated intermediate and ethanol. Mono-de-ethylated dye derivative B can also be adsorbed on the surface of Zn leading to similar events (electron attack, hydrolysis, or deprotonation) that yield bi-de-ethylated dye derivatives, C and D. The *N*-de-ethylation process, as described above, continues until the formation of the complete de-ethylated dye J. The concentrations of the other intermediates are perhaps too low to be examined by HPLC–PDA–ESI–MS. These results can be seen more clearly in Fig. 10.

3.5.2. Destruction of the conjugated structure of the EV

As described above, electrons flow to the EV molecule via the positive diethylamine group. The subsequent transfer of electrons through the conjugated structure yields a carbon-centered radical, which is subsequently attacked by molecular oxygen, resulting ultimately in a and α. The destruction of the conjugated structure of the EV dye most likely occurs through the attack of O_2 on carbon-centered radicals of the EV, as observed in intermediates a–f, isolated from the HPLC chromatogram. This process also occurs in *N*-de-ethylated EV derivatives (B–F) adsorbed on the Zn surface, which implicates electrons in other, similar events (electron attack, hydrolysis or deprotonation, and/or oxygen attack), yielding the mono-*N*-de-ethylated derivative b. A similar process occured in α to produce β. The *N*-de-ethylation process for a and α continued until the formation of the complete *N*-de-ethylated derivatives f and γ. All of the above *N*-de-ethylation processes also produced a series of *N*-de-hydroxyethylated intermediates through the hydroxylation of the *N*-ethyl group. All of the intermediates were further degraded to *N*,*N*-diethylaminobenzene, *N*-ethylaminobenzene, aminobenzene, acetamide, 2-propenoic acid, and acetic acid, which were subsequently mineralized to CO_3^{2-} and NO_3^- [32]. The degradation intermediates clearly reached their maximum concentrations, although some might have remained under the detection limit. Mechanisms similar to those proposed here were also presented in a previous study of the MEK/TiO_2 system [33].

Further evidence regarding the pathway(s) of degradation was obtained by GC–MS spectroscopy. According to the results of mass spectral analysis, the major components in the gas chromatogram were identified as *N*,*N*-diethylaminobenzene, *N*-ethylaminobenzene, aminobenzene, acetamide, 2-propenoic acid, and acetic acid. The former intermediates (**I**–**III**) detected by GC–MS were the result of the cleavage of intermediates of the third group (a–f), leading to aminobenzene derivatives. The latter intermediates (**IV**–**VI**) were formed by the cleavage of aromatic derivatives, leading to aliphatic products. These results can be seen more clearly in Fig. 11.

4. Conclusions

This paper presents the degradation mechanism of ethyl violet dyes, as determined by HPLC–PDA–ESI–MS. This study fabricated a nanostructural ZnO film on the Zn foil of the Alkaline-Manganese dioxide–Zinc Cells. This approach has excellent potential for future applications in the photocatalytic degradation of organic dyes. This study separated and characterized 26 intermediates of the degradation process using HPLC–PDA–ESI–MS and GC–MS. In accor-

dance with variations in the quantity of the intermediates, we also propose possible degradation pathways associated with the decolorization of dyes.

Acknowledgement

This research was supported by the National Science Council of the Republic of China (NSC 97-2113-M-142-002-MY2; NSC 98-2622-M-142-001-CC1).

Appendix A. Supplementary material

Supplementary data associated with this article can be found, in the online version, at http://dx.doi.org/10.1016/j.seppur.2012.06.020.

References

[1] Ullmann's Encyclopedia of Industrial Chemistry. Part A27. Triarylmethane and Diarylmethane Dyes, sixth ed., Wiley-VCH, New York, 2001.
[2] M.A. Fox, D.F. Duxbury, The photochemistry and photophysics of triphenylmethane dyes in solid and liquid media, Chem. Rev. 93 (1993) 381–433.
[3] C.C. Chen, H.J. Fan, J.L. Jan, Degradation pathways and efficiencies of acid blue 1 by photocatalytic reaction with ZnO nanopowder, J. Phys. Chem. C 112 (2008) 11962–11972.
[4] C.C. Chen, C.S. Lu, Mechanistic studies of the photocatalytic degradation of methyl green: an investigation of products of the decomposition processes, Environ. Sci. Technol. 41 (2007) 4389–4396.
[5] B.P. Cho, T. Yang, L.R. Blankenship, J.D. Moody, M. Churchwell, F.A. Bebland, S.J. Culp, Synthesis and characterization of *N*-demethylated metabolites of malachite green and leucomalachite green, Chem. Res. Toxicol. 16 (2003) 285–294.
[6] C.C. Chen, C.S. Lu, Photocatalytic degradation of basic violet 4: degradation efficiency, product distribution, and mechanisms, J. Phys. Chem. C 111 (2007) 13922–13932.
[7] V. Maurino, C. Minero, E. Pelizzetti, P. Piccinini, N. Serpone, H. Hidaka, The fate of organic nitrogen under photocatalytic conditions: degradation of nitrophenols and aminophenols on irradiated TiO_2, J. Photochem. Photobiol. A: Chem. 109 (1997) 171–176.
[8] Y.C. Kong, D.P. Yu, B. Zhang, W. Fang, S.Q. Feng, Ultraviolet-emitting ZnO nanowires synthesized by a physical vapor deposition approach, Appl. Phys. Lett. 78 (2001) 407–409.
[9] S.C. Lyu, Y. Zhang, C.J. Lee, H. Ruh, H.J. Lee, Low-temperature growth of ZnO nanowire array by a simple physical vapor-deposition method, Chem. Mater. 15 (2003) 3294–3299.
[10] Y. Liu, Z.H. Kang, Z.H. Chen, I. Shafiq, J.A. Zapien, I. Bello, W.J. Zhang, S.T. Lee, Synthesis, characterization, and photocatalytic application of different ZnO nanostructures in array configurations, Cryst. Growth Des. 9 (2009) 3222–3227.
[11] X. Li, F. Zhao, J. Fu, X. Yang, J. Wang, C. Liang, M. Wu, Double-sided comb-like ZnO nanostructures and their derivative nanofern arrays grown by a facile metal hydrothermal oxidation route, Cryst. Growth Des. 9 (2009) 409–413.
[12] L.E. Greene, M. Law, J. Goldberger, F. Kim, J.C. Johnson, Y.F. Zhang, R.J. Saykally, P.D. Yang, Low-temperature wafer-scale production of ZnO nanowire arrays, Angew. Chem. Int. Ed. 42 (2003) 3031–3034.
[13] C. Li, G. Hong, P. Wang, D. Yu, L. Qi, Wet chemical approaches to patterned arrays of well-aligned ZnO nanopillars assisted by monolayer colloidal crystals, Chem. Mater. 21 (2009) 891–897.
[14] M.H. Huang, S. Mao, H. Feick, H.Q. Yan, Y.Y. Wu, H. Kind, E. Weber, R. Russo, P.D. Yang, Room-temperature ultraviolet nanowire nanolasers, Science 292 (2001) 1897–1899.
[15] M. Palumbo, T. Lutz, C.E. Giusca, H. Shiozawa, V. Stolojan, D.C. Cox, R.M. Wilson, S.J. Henley, S. Ravi, P. Silva, From stems (and stars) to roses: shape-controlled synthesis of zinc oxide crystals, Cryst. Growth Des. 9 (2009) 3432–3437.
[16] Y. Tak, K. Yong, Controlled growth of well-aligned ZnO nanorod array using a novel solution method, J. Phys. Chem. B 109 (2005) 19263–19269.
[17] M. Mo, D. Wang, X. Du, J. Ma, X. Qian, D. Chen, Y. Qian, Engineering of nanotips in ZnO submicrorods and patterned arrays, Cryst. Growth Des. 9 (2009) 797–802.
[18] Y. Ding, P.X. Gao, Z.L. Wang, Catalyst-nanostructure interfacial lattice mismatch in determining the shape of VLS grown nanowires and nanobelts: a case of Sn/ZnO, J. Am. Chem. Soc. 126 (2004) 2066–2072.
[19] Chong Jia, Xinhua Zhang, Yiqing Chen, Yong Su, Qingtao Zhou, Minjun Xin, Yousheng Lv, Weihai Kong, Liquid phase epitaxial growth and optical property of flower-like ZnO nanosheets on Zinc foil, Appl. Surf. Sci. 254 (2008) 2331–2335.
[20] H. Yu, Z. Zhang, M. Han, X. Hao, F. Zhu, A general low-temperature route for large-scale fabrication of highly oriented ZnO nanorod/nanotube arrays, J. Am. Chem. Soc. 127 (2005) 2378–2379.
[21] B. Cheng, W. Shi, J.M. Russell-Tanner, L. Zhang, E.T. Samulski, Synthesis of variable-aspect-ratio, single-crystalline ZnO nanostructures, Inorg. Chem. 45 (2006) 1208–1214.
[22] C. Wang, E. Shen, E. Wang, L. Gao, Z. Kang, C. Tian, Y. Lan, C. Zhang, Controllable synthesis of ZnO nanocrystals via a surfactant-assisted alcohol thermal process at a low temperature, Mater. Lett. 59 (2005) 2867–2871.
[23] B. Liu, H.C. Zeng, Hydrothermal synthesis of ZnO nanorods in the diameter regime of 50 nm, J. Am. Chem. Soc. 125 (2003) 4430–4431.
[24] A. Dev, S. Kar, S. Chakrabarti, S. Chaudhuri, Optical and field emission properties of ZnO nanorod arrays synthesized on zinc foils by the solvothermal route, Nanotechnology 17 (2006) 1533–1540.
[25] H. Yang, Y. Song, L. Li, J. Ma, D. Chen, S. Mai, H. Zhao, Large-scale growth of highly oriented ZnO nanorod arrays in the Zn–NH_3·H_2O hydrothermal system, Cryst. Growth Des. 8 (2008) 1039–1043.
[26] C. Yan, D. Xue, Conversion of ZnO nanorod arrays into ZnO/ZnS nanocable and ZnS nanotube arrays via an in situ chemistry strategy, J. Phys. Chem. B 110 (2006) 25850–25855.
[27] Y. Wang, X. Li, G. Lu, X. Quan, G. Chen, Highly oriented 1-D ZnO nanorod arrays on zinc foil: direct growth from substrate, optical properties and photocatalytic activities, J. Phys. Chem. C 112 (2008) 7332–7336.
[28] L.S. Panchakarla, A. Govindaraj, C.N.R. Rao, Formation of ZnO nanoparticles by the reaction of zinc metal with aliphatic alcohols, J. Clust. Sci. 18 (2007) 660–670.
[29] A. Zuttel, Hydrogen storage methods, Naturwissenschaften 91 (2004) 157–172.
[30] L.S. Panchakarla, M.A. Shah, A. Govindaraj, C.N.R. Rao, A simple method to prepare ZnO and $Al(OH)_3$ nanorods by the reaction of the metals with liquid water, J. Solid State Chem. 180 (2007) 3106–3110.
[31] C. Yan, D. Xue, Solution growth of nano- to microscopic ZnO on Zn, J. Cryst. Growth 310 (2008) 1836–1840.
[32] A.B. Prevot, C. Baiocchi, M.C. Brussino, E. Pramauro, P. Savarino, V. Augugliaro, G. Marci, L. Palmisano, Photocatalytic degradation of acid blue 80 in aqueous solutions containing TiO_2 suspensions, Environ. Sci. Technol. 35 (2001) 971–976.
[33] F.D. Mai, C.C. Chen, J.L. Chen, S.C. Liu, Photodegradation of methyl green using visible irradiation in ZnO suspensions: determination of the reaction pathway and identification of intermediates by a high-performance liquid chromatography–photodiode array–electrospray ionization–mass spectrometry method, J. Chromatogr. A 1189 (2008) 355–365.